frontiers | Frontiers in Astronomy and Space Sciences

TYPE Original Research
PUBLISHED 24 April 2023
DOI 10.3389/fspas.2023.1162005

OPEN ACCESS

EDITED BY
Ludmila Carone,
Austrian Academy of Sciences, Austria

REVIEWED BY
Xiaohua Fang,
University of Colorado Boulder,
United States
Vincent N. Génot,
UMR5277 Institut de recherche en astrophysique et planétologie (IRAP),
France

*CORRESPONDENCE
Yun Li,
liyunbuaa@buaa.edu.cn

RECEIVED 09 February 2023
ACCEPTED 11 April 2023
PUBLISHED 24 April 2023

CITATION
Li G, Lu H, Li Y, Song Y, Cao J and Li S (2023), Influence of the Martian crustal magnetic fields on the Mars-solar wind interaction and plasma transport. *Front. Astron. Space Sci.* 10:1162005. doi: 10.3389/fspas.2023.1162005

Influence of the Martian crustal magnetic fields on the Mars-solar wind interaction and plasma transport

Guokan Li[1], Haoyu Lu[1,2], Yun Li[1,2]*, Yihui Song[1], Jinbin Cao[1,2] and Shibang Li[1]

[1]School of Space and Environment, Beihang University, Beijing, China, [2]Key Laboratory of Space Environment Monitoring and Information Processing, Ministry of Industry and Information Technology, Beijing, China

The plasma transport process is important for the ionosphere of Mars, which controls the structure of the ionosphere above an altitude of 200 km. Plasma transport from the dayside ionosphere is crucial for producing the nightside ionosphere on Mars. The alteration in dayside plasma transport in the presence of crustal fields may influence the distribution of Martian ionospheric plasma and plasma escape in the magnetotail. This study employed a three-dimensional multispecies magnetohydrodynamic (MHD) model to simulate Mars-solar wind interactions. We show the magnetic field distribution and plasma velocity variation on the Martian day-side. The results indicate that the ion transport from low- to high-solar-zenith-angle areas in the south is inhibited by crustal fields, leading to a reduction in the ion number density and a thinner ionosphere near the southern terminator. Many heavy ions remain in the southern dayside ionosphere rather than moving to the nightside. In addition, the maximum reduction in the tailward flux of the planetary ions calculated by the MHD simulation is more than 50% at the southern terminator, indicating an inhibitory effect of the crustal fields on day-to-night transport. These effects may lead to a reduction in ion number density in the southern nightside ionosphere. Finally, we demonstrate a decrease in the global heavy-ion loss rate.

KEYWORDS

crustal magnetic fields, three-dimensional multispecies magnetohydrodynamic model, Mars-solar wind interactions, plasma transport, ion escape

1 Introduction

Mars is an unmagnetized planet; thus, the coupling processes of the magnetosphere-ionosphere system on Mars and Earth are different (Nagy et al., 2004; Yao et al., 2017). The solar wind directly interacts with the ionosphere and upper atmosphere of Mars, partly magnetizing the ionosphere and picking up exospheric particles under the variable interplanetary magnetic field (IMF) orientation (Liu et al., 2020; Liu et al., 2021). On the other hand, there are complex local crustal magnetic fields on the surface of Mars, which are primarily distributed in the southern hemisphere (Acuña et al., 1998; Connerney et al., 2005; Connerney et al., 2015). Therefore, a complicated and dynamic magnetic system occurs during the interactions between Mars and solar winds (Weber et al., 2017; Weber at al., 2020; Xu et al., 2017; Xu et al., 2019; Zhang et al., 2022). This magnetic system controls the transport of mass, energy, and momentum between Mars

and solar winds (Xu et al., 2018; Weber et al., 2020), including reconnection, magnetospheric boundary formation, energetic electron precipitation, and low-energy ion outflow and pick-up, which leads to alterations in the plasma boundary locations (Brain et al., 2005; Edberg et al., 2008; Edberg et al., 2009; Xu et al., 2016; Fang et al., 2017; Garnier et al., 2022), heating (Cui et al., 2018), and exerting inhibiting or promoting effects on the plasma transport process (Brain et al., 2006; Lundin et al., 2006; Lundin et al., 2011; Fang et al., 2015).

The structure of the dayside magnetosphere is directly controlled by magnetized solar winds and local crustal sources (Ulusen et al., 2016; Luhmann et al., 2017; Weber et al., 2019; Weber et al., 2020). Different magnetic topologies exist in the dayside of the magnetosphere. Recent observational study reported seven magnetic topologies in the Martian plasma environment, with three types mainly existing on the dayside: closed (connected only to Mars), open (connected to both Mars and solar winds), and draped (connected only to solar winds) (Weber et al., 2017; Xu et al., 2017; Xu et al., 2019). As strong crustal field sources are primarily distributed in the Southern Hemisphere, the distribution of the magnetic topology presents an obvious north-south asymmetry. On the day, different magnetic field lines control the horizontal or radial plasma transport, altering the planetary ion escape rates and the location of the plasma boundaries (Matta et al., 2015; Dubinin et al., 2019; Li et al., 2022a). The plasma transport process is important in the ionosphere of Mars. It controls the structure of the ionosphere above an altitude of 200 km, as well as the location of the dayside ionopause. Plasma transport from the dayside ionosphere is an important source for the nightside ionosphere (Cui et al., 2015; Girazian et al., 2017; Adams et al., 2018; Cao et al., 2019). Observational studies have reported an upward spread of the ionosphere and an increase in the O^+ flux in the southern hemisphere (Lundin et al., 2011; Dubinin et al., 2019). Moreover, the tailward transport of heavy ions from the southern hemisphere strongly deviates near the terminator rather than flowing to the magnetotail (Lundin et al., 2011; Cao et al., 2019), resulting in decreased heavy ion loss rates in the magnetotail (Fang et al., 2015; Ma et al., 2015). Previous studies have summarized the above influences as a shielding effect of the crustal fields on the dayside ionosphere, which protects the plasma from penetrating the solar wind and IMF (Brain et al., 2010; Nilsson et al., 2011; Inui et al., 2021). However, the mechanism of this shielding effect is not completely understood. Based on published observations by the Mars Global Surveyor, Mars Express, and Mars Atmosphere and Volatile Evolution missions, a detailed quantitative description of heavy-ion transport in the dayside ionosphere is required.

In this study, a multispecies magnetohydrodynamic (MHD) numerical model was adopted to simulate the solar-wind interaction with Mars. The 110° spherical harmonic model developed by Gao et al. (2021) was used to describe the crustal fields. We describe the vertical and horizontal plasma motion around the quasi-spherical ionosphere and calculate the distribution of planetary ions and the tailward ion flux across the terminator plane. These results are conducive to understanding the role of crustal fields in day-to-night plasma transport.

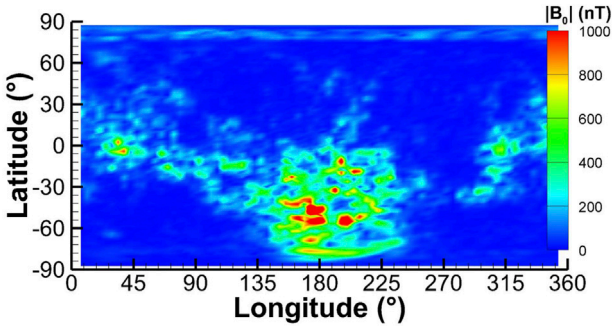

FIGURE 1
Distributions of the crustal field strength at the altitude of 100 km calculated by the 110° spherical harmonic model developed by Gao et al. (2021).

2 Method

We employed a three-dimensional multispecies MHD model to simulate Mars-solar-wind interaction. The model includes a set of four continuity equations for the ion species (H^+, O_2^+, O^+, and CO_2^+), with the highest contributions in the Martian ionosphere. A set of eight-wave MHD equations were used in the model, augmented with a series of ionospheric chemical reactions, including photoionization, ion-neutral reactions, and dissociative recombination. The model was based on the formalism proposed by Ma et al. (2004), which integrated the MHD equations with the mass conservation equation for individual ion species. In our model, the mass equations for the four ion species are decoupled from the main MHD equations to facilitate the implementation of the calculation (Li et al., 2021). The decoupled MHD equations, as well as the details of the model setup, refer to the model of Li et al. (2021), which has been shown to roughly describe the plasma environment in the Mars-solar wind interaction without crustal fields. In our model, the total number of cells in the whole simulation domain was 960000, with the highest radial resolution reaching 10 km near the inner boundary (100 km) to accurately calculate the structure of the ionosphere (Ma et al., 2004; Fang et al., 2015). The resolutions of the Mars Solar Orbital (MSO) longitude and latitude were 3.6° and 4.5°, respectively. The program was parallelized to improve the computing speed. Moreover, the photoionization effect was included by adopting the Chapman function method (Huestis, 2001), which has been shown to significantly improve agreement with plasma density observations (Withers, 2009). Our calculations were performed in the Mars Solar Orbital coordinate system, with the x-axis pointing from Mars toward the Sun, the z-axis perpendicular to the x-axis and parallel to the northward normal of the orbital plane of Mars, and the y-axis completing the right-handed coordinate system. The simulation domain was within—24 $R_M \leq x \leq 8$ R_M and—16 $R_M \leq y, z \leq 16$ R_M, where R_M is the radius of Mars (3,396 km). The inner boundary of the grid was set 100 km above the Martian surface. The density and speed of the upstream solar wind were 4–3 cm and 400 km/s, respectively. The IMF is assumed to be along the nominal Parker spiral, as specified by $|B| = 3$ nT and $(B_X, B_Y, B_Z) = (-1.6, 2.5, 0)$ nT.

10.3389/fspas.2023.1162005

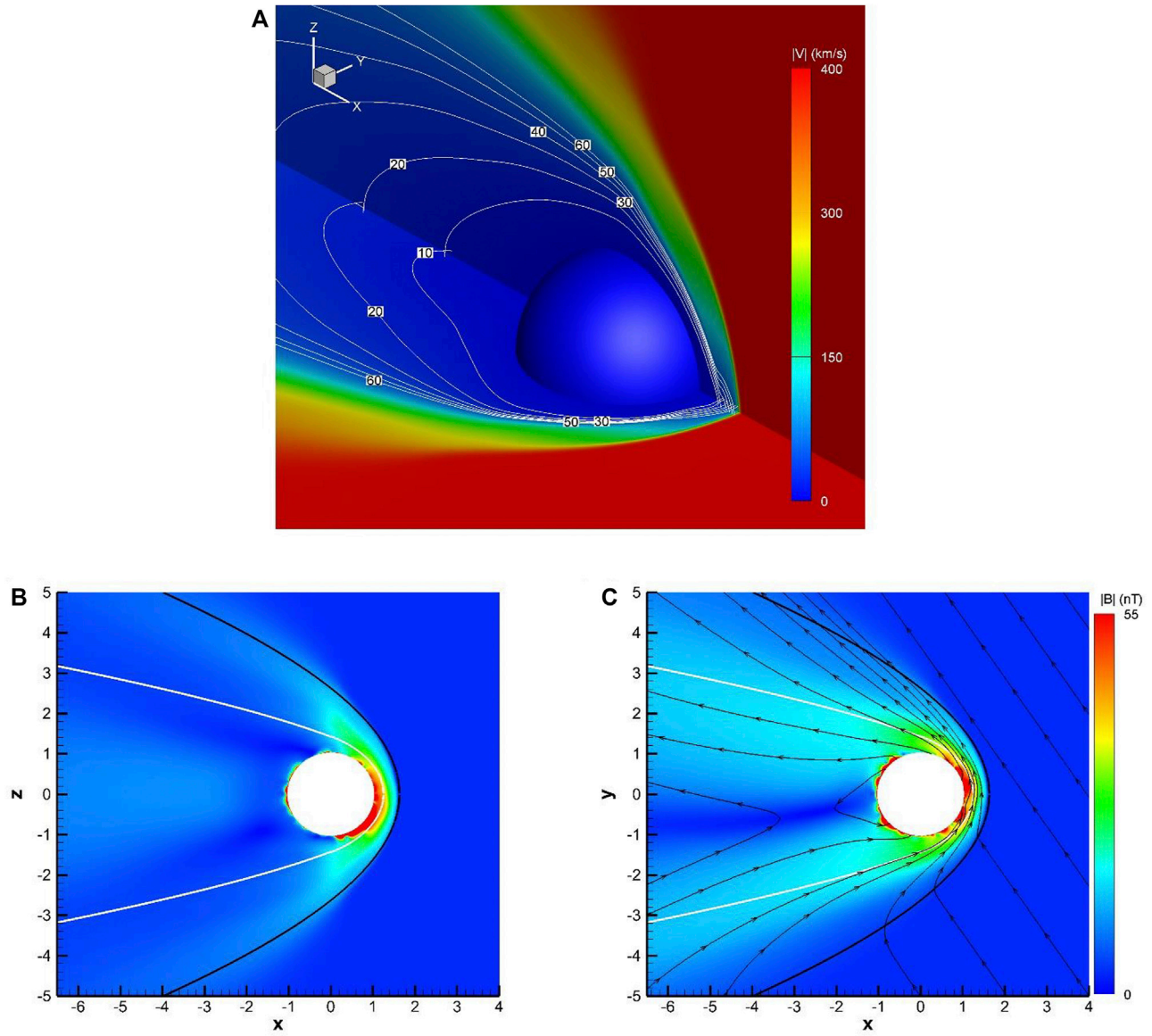

FIGURE 2
(A) Distributions of the plasma velocity in the x-y and x-z plane. The blue spherical surface is the inner boundary of the model. The white lines with labels are the isocontours of |V| = 10–60 km; **(B, C)** Distributions of the magnetic field in the x-z **(B)** and x-y **(C)** plane. White and black solid quasi-parabolas represent the mean locations of MPB and BS from Vignes et al. (2000), respectively. The black curves with arrows in **(C)** is the magnetic field lines.

In this study, the 110° spherical harmonic model developed by Gao et al. (2021) was included, as it has been demonstrated in detail to describe the crustal magnetic fields of Mars. Figure 1 presents the distributions of the crustal field strength at the altitude of 100 km. As shown in Figure 1, all the strong crustal field sources, with a magnetic field strength of > 10^3 nT on the inner boundary of the model, are located predominantly in the southern hemisphere. The strongest source is located near 45°S and 180°W. However, the crustal field sources in the north are weak, with a magnetic field strength < 200 nT near the inner boundary of the model. A case without a crustal field was also used as a control group to clearly demonstrate the effects of crustal fields. Finally, the subsolar location was set at 180°W and 0°N.

3 Results

Figure 2A shows the distribution of the plasma velocity (|V|) in the X-Y and X-Z planes. In Figure 2A, the location where the impacting solar winds suddenly decelerate in front of Mars represents the location of the bow shock (BS). The solar wind plasma flow is deflected, crosses the terminator, and then flows downstream. The plasma velocity in the near-Mars region is significantly lower than that outside the BS. The shapes of the velocity isocontours show that the low-velocity region increases from the subsolar point to the terminator and nightside. Figures 2B, C show the distribution of the calculated magnetic field (|B|) in the x-y and x-z planes. Magnetic field B was obtained from the vector

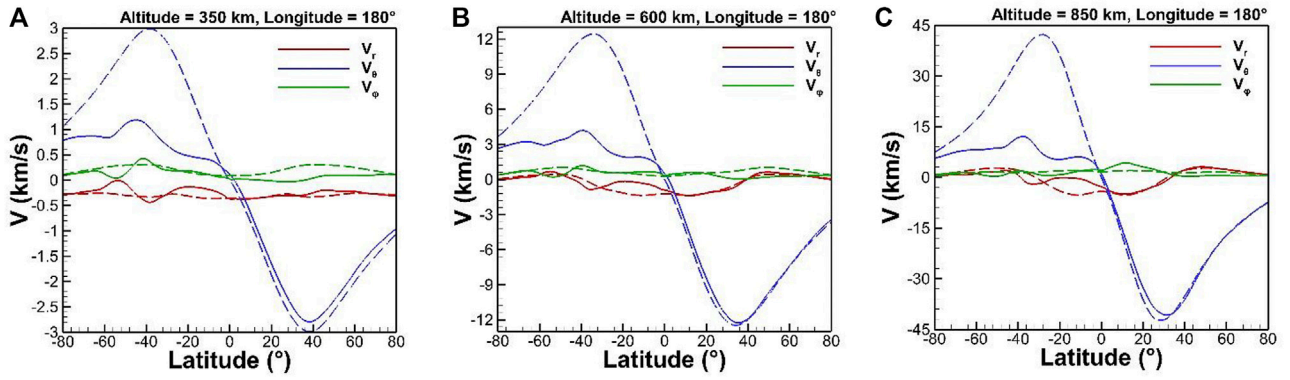

FIGURE 3
V_r, V_θ, and V_φ along the 180°W MSO longitude line at different altitudes. **(A)** 350 km; **(B)** 600 km; **(C)** 850 km. Solid/Dashed lines represent the case with/without the crustal fields.

sum of the induced and crustal magnetic fields. On the dayside, the magnetic field jumps from a low background value (3 nT, blue area in the Figure) to approximately 10 nT (green area), representing the location of the BS. The magnetic pile-up region can be characterized by areas colored yellow and red. Owing to the existence of crustal fields, the southern magnetosphere expands in the middle SZA area. At night, the draped and extended field lines form an induced magnetotail with a double-lobe structure. The magnetic field and velocity are self-consistently calculated and concur with previous investigations (Nagy et al., 2004; Li et al., 2021).

Owing to the significant north-south asymmetry in the magnetic field strength distribution, the plasma motion pattern may be different in the northern and southern hemispheres. Figure 3 shows the variations in V_r, V_θ, and V_φ at altitudes of 350, 600, and 850 km and MSO longitudes of 180°W. In this study, V_r is the radial velocity with the positive direction pointing away from Mars. The positive direction of V_θ is along the tangent of any longitudinal line and points to the south, and the positive direction of V_φ is obtained by the right-hand rule based on the positive directions of V_r and V_θ. The altitude of 350 km is close to the average ionopause height reported by Chu et al. (2019) and Sánchez-Cano et al. (2020). In most cases, the altitude of 600 km is higher than the ionopause height in most of the cases (Duru et al., 2020). An altitude of 850 km is close to the average height of the magnetic pileup boundary (MPB) above the subsolar point (Li et al., 2020; Li et al., 2021). As shown in Figure 3, the mean magnitude and peak values of V_θ are higher than V_r and V_φ. In the near-terminator region, owing to the extension of the low-velocity region (as shown in Figure 1A), the value of V_θ significantly decreases. This result indicates that the high-speed plasma flow is farther away from the Mars in the near-terminator region than on the dayside. The southern V_θ peaks represented by solid lines (with crustal fields) were significantly lower than those represented by dashed lines (without crustal fields) by 60%, 66.7%, and 72.1%, respectively. Additionally, the northern peak value of the red lines is 5% lower than that of the blue lines. However, the magnitude variations in V_r and V_φ above the strong crustal sources in the southern hemisphere are not obvious. Owing to the reduction in V_θ and local increases and decreases in both V_r and V_φ, the moving directions of the plasma flow in the southern hemisphere are more complex, and day-to-night plasma transport is inhibited. Lundin et al. (2011) reported that in the presence of crustal fields, the moving directions of the unit flow vectors near 180°W are disordered in the southern hemisphere, whereas those in the northern hemisphere move directly toward the nightside along the meridional direction. The similar conclusions between Lundin et al. (2011) and our study indicates an important controlling effect of crustal fields on plasma motion.

Figure 3 indicates that in the southern hemisphere, many heavy ions remain in the low- and middle-solar-zenith-angle (SZA) areas rather than reaching the terminator. This effect may result in upward expansion of the ionosphere in these SZA areas. Figure 4 shows the distribution of the logarithmic number densities of O_2^+, O^+, and CO_2^+ in the SZA-altitude coordinate system. The data used in Figure 4 is extracted from the x-z plane of the model results. In the case of crustal fields, the distribution areas of planetary ions extend to higher altitudes in the SZA range of 0°–60°. However, in the SZA range of 60°–90°, the green areas (the number density of O^+ is more than 10^1, or the number density of O_2^+ and CO_2^+ is more than 10^2), as shown in Figures 4D–F. This result indicates that the alteration in ion number density near the terminator may be opposite to that occurring in the low- and middle-SZA areas. To clarify the variation in the number density distributions of O_2^+, O^+, and CO_2^+ in the southern and northern hemispheres. Figure 5 shows the distributions of the logarithmic number densities of O_2^+, O^+, and CO_2^+ in the x-z plane. In the presence of crustal fields, the extension of the distribution area of planetary ions mainly occurs in the low- and middle-SZA areas of the southern hemisphere. This result indicates that the ionosphere expands above strong crustal sources (Duru et al., 2006; Duru et al., 2020; Sánchez-Cano et al., 2020). Shrinking of the high-number-density regions of the planetary ions is observed near the southern terminator. Figure 5 indicates that the variation in the number density distribution in Figure 4 mainly occurs in the southern hemisphere.

To verify the change in the ion number density near the southern terminator, isocontours of the logarithmic planetary ion number density on the x-z plane and the southern terminator are shown in Figure 6. From inside to outside, the four isocontours represent the locations $n_{total} = 10^3$, 10^2, 10^1, 10^0, respectively. In the

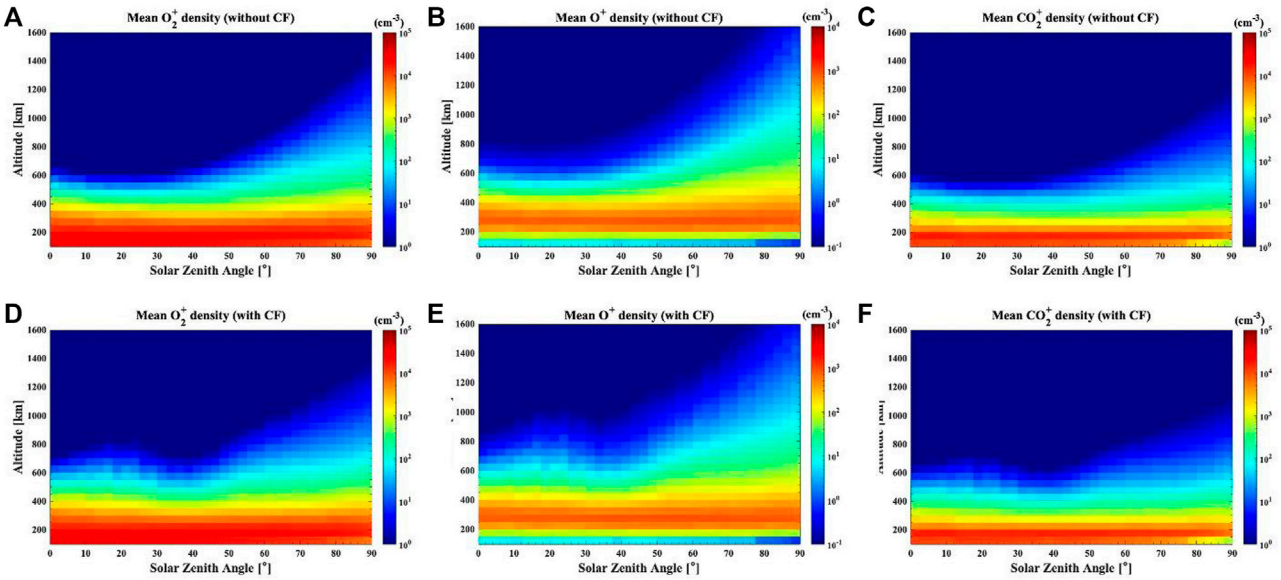

FIGURE 4
The distributions of the logarithmic number density of O_2^+ **(A, D)**, O^+ **(B, E)**, and CO_2^+ (c. f) in the SZA-Altitude coordinate system, in the case without **(A–C)** and with **(D–F)** crustal fields.

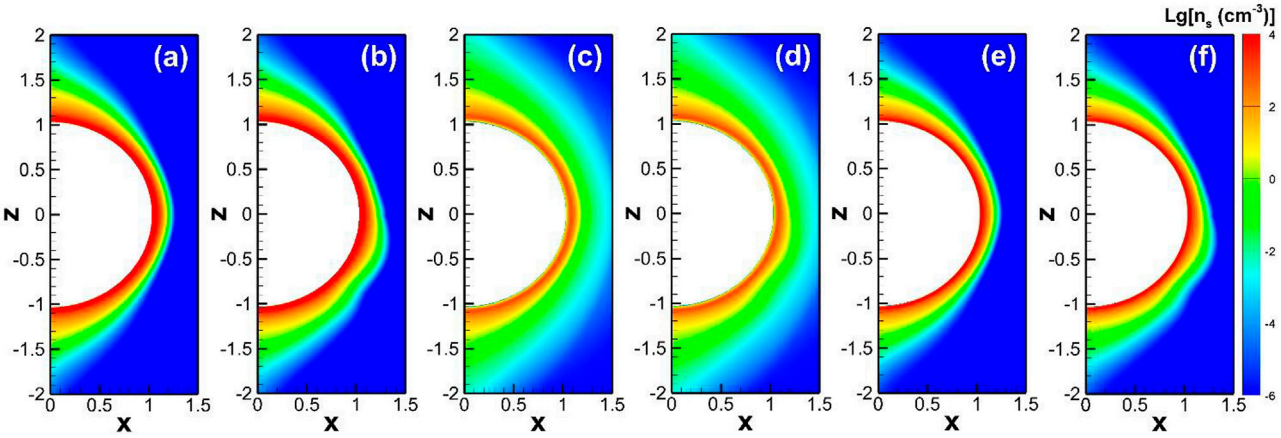

FIGURE 5
The dayside distributions of the logarithmic number density of O_2^+ **(A, B)**, O^+ **(C, D)**, and CO_2^+ (e. f) in the x-z plane, in the case without **(A, C, E)** and with **(B, D, F)** crustal fields.

presence of crustal fields, the altitudes of the isocontours (red lines) in Figure 6A increase in the low- and middle-SZA areas and decrease in the high-SZA area. Figure 6B shows that on the terminator, the ionosphere shrinks in most SZA areas. These results indicate a reduction in the ion number density transported from the low- and middle-SZA areas to the high-SZA areas under the influence of crustal fields. The variation in the ion number density in Figures 4–6 mainly occurs at altitudes of 600–1000 km (about 1.2–1.35 R_M). At higher altitudes, variations in ion number density were not obvious.

Owing to the decrease in V_θ in the southern hemisphere and the reduction in the ion number density near the southern terminator, day-to-night transport across the southern terminator is inhibited. Figure 7 shows the flux-altitude distribution of the tailward planetary ion flux (Q_X) at all grid points on the terminator. The points in the cases with and without crustal fields are colored in red and blue, respectively. In the northern hemisphere (Figure 7A), the tailward flux distribution of planetary ions is similar in the two cases. However, in the southern hemisphere (Figure 7B), the tailward fluxes shown by the red points are lower above an altitude of 300 km. As the altitude increases, the reduction in the tailward flux of planetary ions is more than 14% above 300 km altitude and reaches 50% above 800 km altitude. This effect may result in a

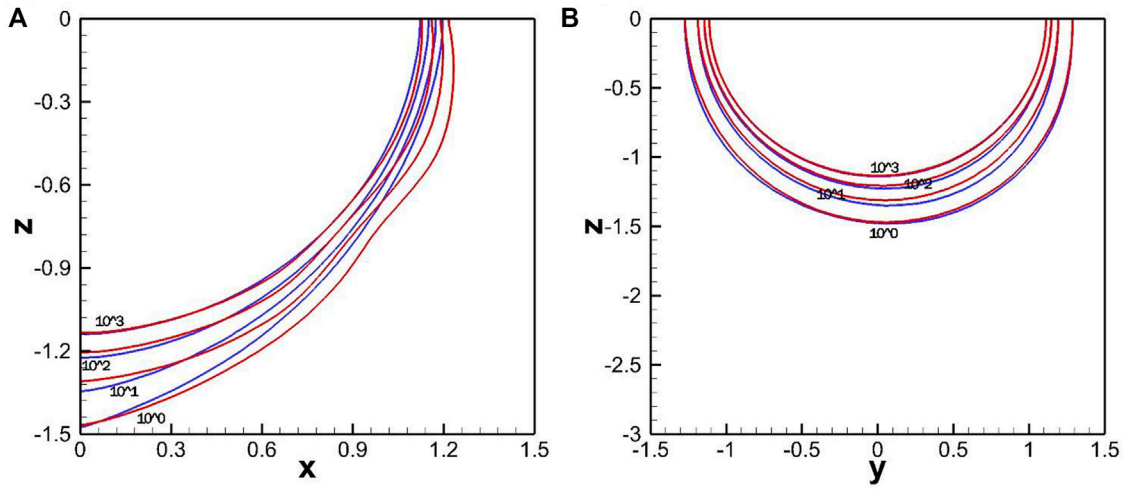

FIGURE 6
The isocontours of the logarithmic planetary ion number density on the southern x-z plane **(A)** and southern terminator **(B)**. Red/blue line represents the case with/without crustal fields.

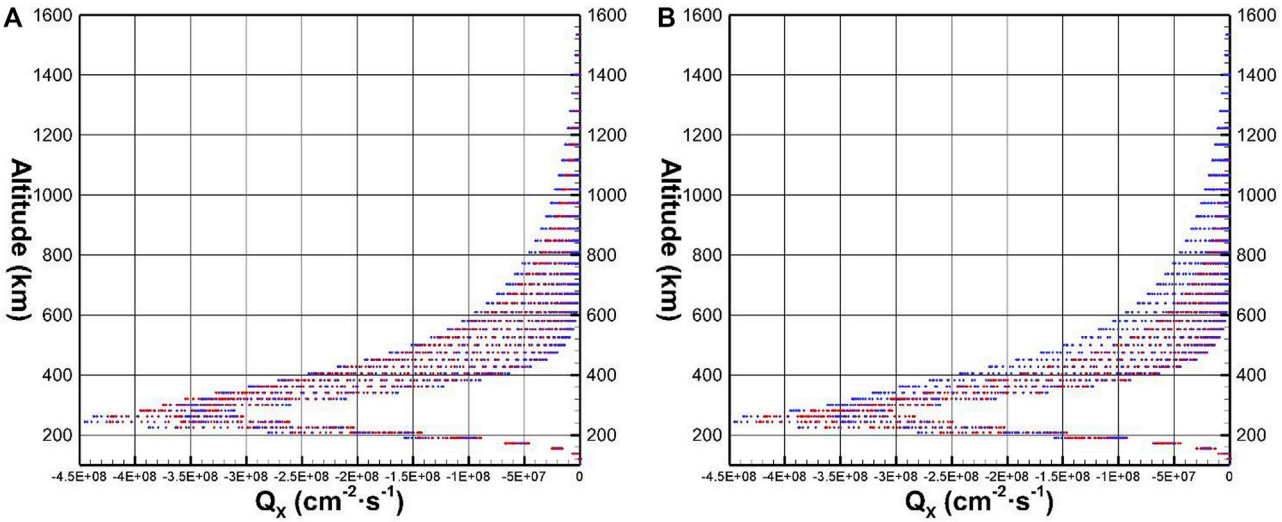

FIGURE 7
Variations in the tailward ion flux escaping through the grid points in the northern **(A)** and southern **(B)** hemisphere with the altitude. Red/Blue points represent the case with/without the crustal fields.

TABLE 1 The global loss rates of O_2^+, O^+, and CO_2^+ in cases with and without crustal fields.

Ion species	With crustal fields (s^{-1})	Without crustal fields (s^{-1})
O_2^+	8.17×10^{21}	1.09×10^{22}
O^+	1.49×10^{23}	1.65×10^{23}
CO_2^+	4.06×10^{21}	5.16×10^{21}

thinner nightside ionosphere in the southern hemisphere, which consequently leads to a decrease in the loss rate of planetary ions from the southern magnetotail. Finally, Table 1 lists the calculated global loss rates of O_2^+, O^+, and CO_2^+ at 6 R_M. In the presence of crustal fields, reductions in the global loss rates of O_2^+, O^+, and CO_2^+ were 25%, 9.7%, and 21.3%, respectively. Although the open

magnetic field lines on the dayside may promote upward plasma motion and increase the ion loss rate (Li et al., 2022a), Table 1 indicates that the reduction in the global loss rate is strongly related to the reduction in the tailward flux.

4 Summary and discussion

This study investigated the influence of the Martian crustal magnetic field on dayside and day-to-night plasma transport and its potential influence on the tailward escape processes of heavy ions. The latest 110° spherical harmonic model developed by Gao et al. (2021) was used to calculate crustal fields. Our simulation results concur with those of previous investigations, indicating that our model can self-consistently calculate plasma and field environments during interactions between Mars and solar winds. In this study, spherical coordinate velocity components were adopted to describe plasma motion in the dayside ionosphere more appropriately. Our results indicate the dominance of the meridional velocity V_θ in the dayside plasma motion and showed a significant decrease under the influence of crustal fields. Finally, we show the reduction in the ion number density and tailward flux near the southern terminator, as well as the reduction in the global ion loss rates in the presence of crustal fields.

The mechanism by which crustal fields affect- the solar wind interaction is still an important issue. This study provides a new aspect of the mechanism of the shielding effect, relating the altered ionosphere structure and reduced tailward plasma escape to meridional plasma transport on the dayside. In this study, the tilt of the rotational axis (approximately 25°) is ignored. When an oblique rotational axis of Mars is considered, the subsolar point is located in the northern and southern hemispheres in different seasons, and the relevant location between the strongest crustal source and solar wind inflow changes. When the subsolar point is located in the northern hemisphere, the strongest crustal source approaches the southern end. Therefore, the shielding effect is weaker, and the tailward plasma escape is enhanced (Ma et al., 2014; Fang et al., 2017). On the other hand, when the subsolar point is located in the southern hemisphere, the strongest crustal source approaches the subsolar point, and the north-south asymmetry in plasma transport is not obvious. Consequently, to reveal an apparent north-south asymmetry in plasma transport, the strongest crustal source was set to face the Sun.

Furthermore, Mars-solar wind interactions are dynamic and influenced by the rotation of crustal fields with Mars, which was ignored in this study (Ma et al., 2014; Li et al., 2021; Liu et al., 2021). Time-dependent MHD simulations have indicated that the response of the variation in the ion loss rate to the rotation of crustal fields has a 3-h delay (Fang et al., 2015). When the strongest crustal source faces the Sun, the inhibitory effect is the most obvious. However, the crustal source near the terminator leads to an escape-fostering effect and increases the ion loss rate (Fang et al., 2017). Therefore, the static model may underestimate the ion loss. The crustal fields also result in a twisting effect on the structure of the current sheet in the magnetotail (DiBraccio et al., 2018; DiBraccio et al., 2022). The influence of the twist structure on tailward ion escape is not fully understood. The conclusions of this study are conducive to understanding the north-south asymmetry of heavy-ion escape under the influence of crustal fields. Based on the results of the velocity and ion distributions, this study will contribute to understanding the mechanism by which the complex distributed crustal fields alter the plasma environment of Mars.

5 Conclusion

Owing to the north-south asymmetry in the distribution of crustal fields on Mars, the magnetic structures also differ significantly between north and south. In the presence of strong crustal sources, enhanced closed and open fields occur in the southern hemisphere, which exert an influence even at high altitudes, controlling plasma motion and altering the position of the plasma boundary (Fang et al., 2017; Li et al., 2022a; Li et al., 2022b). In contrast, because of the lack of strong crustal fields in the northern hemisphere, the plasma environments are similar to those on unmagnetized planets, with the magnetic structure and plasma motion primarily controlled by the draped IMF. Consequently, the patterns of plasma motion are more complex in the south.

Although crustal fields exert both shielding and promoting effects on plasma escape, the shielding effect is dominant when the subsolar point is located at (180°W, 0°N) (Ma et al., 2014). Published studies have indicated that strong crustal field sources provide enhanced magnetic pressure on the dayside ionosphere, counterbalancing the forces exerted by the solar wind plasma and protecting planetary ions from the solar wind (Crider and Dana., 2002; Bertucci et al., 2003; Fang et al., 2015). Previous studies have discussed the variation in dayside radial transport under the influence of crustal fields and the influence on plasma escape (Matta et al., 2015; Li et al., 2022a; Li et al., 2022b). This study demonstrates that when the strongest crustal source faces the Sun, the shielding effect forces the planetary ions to remain in the middle-SZA areas (Lundin et al., 2011; Dubinin et al., 2019; Fowler et al., 2022). In the presence of crustal fields, plasma transport from the low- to high-SZA areas is inhibited owing to the reduced meridional velocity in the southern hemisphere, resulting in a reduction in the ion number density and a reduction in the ionosphere in the southern high-SZA area. The reduction in the tailward flux of planetary ions indicates the inhibition of day-to-night transport. This effect leads to a reduction in the ion number density in the southern nightside ionosphere (Cao et al., 2019), and eventually inhibits planetary ion escape on the southern magnetotail. Consequently, the north-south asymmetrical ionosphere structure and plasma tailward flux are significantly associated with controlled plasma motion by complex distributed crustal fields.

Data availability statement

The raw data supporting the conclusion of this article will be made available by the authors, without undue reservation.

Author contributions

GL, YL, and HL contributed to conception and design of the study. GL and HL organized the database. GL and YL performed the

statistical analysis. GL wrote the first draft of the manuscript. All authors contributed to manuscript revision, read, and approved the submitted version.

Funding

This work was supported by the B-type Strategic Priority Program of the Chinese Academy of Sciences (Grant No. XDB41000000), and the National Natural Science Foundation of China (NSFC) under grant No. 42241114, 42074214, and 12150008, and the pre-research projects on Civil Aerospace Technologies No. D020103 and D020105 funded by China's National Space Administration (CNSA).

Conflict of interest

The authors declare that the research was conducted in the absence of any commercial or financial relationships that could be construed as a potential conflict of interest.

Publisher's note

References

Acuña, M. H., Connerney, J. E. P., Wasilewski, P., Lin, R. P., Anderson, K. A., Carlson, C. W., et al. (1998). Magnetic field and plasma observations at mars: Initial results of the mars global surveyor mission. *Science* 279, 1676–1680. doi:10.1126/science.279.5357.1676

Adams, D., Xu, S., Mitchell, D. L., Lillis, R. J., Fillingim, M., Andersson, L., et al. (2018). Using magnetic topology to probe the sources of Mars' nightside ionosphere. *Geophys. Res. Lett.* 45 (12), 197. doi:10.1029/2018GL080629

Bertucci, C., Mazelle, C., Crider, D. H., Vignes, D., Acuña, M. H., Mitchell, D. L., et al. (2003). Magnetic field draping enhancement at the martian magnetic pileup boundary from Mars global surveyor observations. *Geophys. Res. Lett.* 30 (2), 71. doi:10.1029/2002gl015713

Brain, D. A., Baker, A. H., Briggs, J., Eastwood, J. P., Halekas, J. S., and Phan, T. D. (2010). Episodic detachment of martian crustal magnetic fields leading to bulk atmospheric plasma escape. *Geophys. Res. Lett.* 37 (14). doi:10.1029/2010gl043916

Brain, D. A., Halekas, J. S., Lillis, R., Mitchell, D. L., Lin, R. P., and Crider, D. H. (2005). Variability of the altitude of the martian sheath. *Geophys. Res. Lett.* 32 (18), 109–127. doi:10.1029/2005gl023126

Brain, D. A., Halekas, J. S., Peticolas, L. M., Lin, R. P., Luhmann, J. G., Mitchell, D. L., et al. (2006). On the origin of aurorae on Mars. *Geophys. Res. Lett.* 33 (1). doi:10.1029/2005gl024782

Cao, Y.-T., Cui, J., Wu, X., Guo, J., and Wei, Y. (2019). Structural variability of the nightside martian ionosphere near the terminator: Implications on plasma sources. *J. Geophys. Res. Planets* 124 (6), 1511. doi:10.1029/2019JE005970

Chu, F., Girazian, Z., Gurnett, D. A., Morgan, D. D., Halekas, J., Kopf, A. J., et al. (2019). The effects of crustal magnetic fields and solar EUV flux on ionopause formation at Mars. *Geophys. Res. Lett.* 46, 10257–10266. doi:10.1029/2019GL083499

Connerney, J., Acuña, M. H., Ness, N. F., Kletetschka, G., Mitchell, D. L., Lin, R. P., et al. (2005). From the cover: Tectonic implications of Mars crustal magnetism. *Proc. Natl. Acad. Sci. U. S. A.* 102 (42), 14970–14975. doi:10.1073/pnas.0507469102

Connerney, J. E. P., Espley, J. R., DiBraccio, G. A., Gruesbeck, J. R., Oliversen, R. J., Mitchell, D. L., et al. (2015). First results of the MAVEN magnetic field investigation. *Geophys. Res. Lett.* 42, 8819–8827. doi:10.1002/2015GL065366

Crider, D. H., and Dana, H. (2002). Observations of the latitude dependence of the location of the martian magnetic pileup boundary. *Geophys. Res. Lett.* 29 (8), 11. doi:10.1029/2001GL013860

Cui, J., Galand, M., Yelle, R. V., Wei, Y., and Zhang, S. J. (2015). Day-to-night transport in the Martian ionosphere: Implications from total electron content measurements. *J. Geophys. Res. Space Phys.* 120, 2333–2346. doi:10.1002/2014JA020788

Cui, J., Yelle, R. V., Zhao, L. L., Stone, S., Jiang, F. Y., Cao, Y. T., et al. (2018). The impact of crustal magnetic fields on the thermal structure of the martian upper atmosphere. *Astrophysical J. Lett.* 853 (2), L33. doi:10.3847/2041-8213/aaa89a

DiBraccio, G. A., Luhmann, J. G., Curry, S. M., Espley, J. R., Xu, S., Mitchell, D. L., et al. (2018). The twisted configuration of the martian magnetotail: MAVEN observations. *Geophys. Res. Lett.* 45 (10), 4559. doi:10.1029/2018GL077251

DiBraccio, G. A., Romanelli, N., Bowers, C. F., Gruesbeck, J. R., Halekas, J. S., Ruhunusiri, S., et al. (2022). A statistical investigation of factors influencing the magnetotail twist at mars. *Geophys. Res. Lett.* 49 (12), e2022GL098007. doi:10.1029/2022GL098007

Dubinin, E., Fraenz, M., Pätzold, M., Woch, J., McFadden, J., Halekas, J. S., et al. (2019). Expansion and shrinking of the martian topside ionosphere. *J. Geophys. Res. Space Phys.* 124 (11), 9725–9738. doi:10.1029/2019ja027077

Duru, F., Baker, N., De Boer, M., Chamberlain, A., Verchimak, R., Morgan, D. D., et al. (2020). Martian ionopause boundary: Coincidence with photoelectron boundary and response to internal and external drivers. *J. Geophys. Res. Space Phys.* 125 (5). doi:10.1029/2019JA027409

Duru, F., Gurnett, D. A., Averkamp, T. F., Kirchner, D. L., Huff, R. L., Persoon, A. M., et al. (2006). Magnetically controlled structures in the ionosphere of Mars. *J. Geophys. Res. Space Phys.* 111 (12), A12204. doi:10.1029/2006JA011975

Edberg, N. J. T., Brain, D. A., Lester, M., Cowley, S. W. H., Modolo, R., Fränz, M., et al. (2009). Plasma boundary variability at Mars as observed by Mars global surveyor and Mars express. *Ann. Geophys.* 27 (9), 3537–3550. doi:10.5194/angeo-27-3537-2009

Edberg, N. J. T., Lester, M., Cowley, S. W. H., and Eriksson, A. I. (2008). Statistical analysis of the location of the Martian magnetic pileup boundary and bow shock and the influence of crustal magnetic fields. *J. Geophys. Res.* 113, A08206. doi:10.1029/2008JA013096

Fang, X., Ma, Y., Brain, D., Dong, Y., and Lillis, R. (2015). Control of Mars global atmospheric loss by the continuous rotation of the crustal magnetic field: A time-dependent mhd study. *J. Geophys. Res. Space Phys.* 120 (12), 10,926. doi:10.1002/2015ja021605

Fang, X., Ma, Y., Masunaga, K., Dong, Y., Brain, D., Halekas, J., et al. (2017). The Mars crustal magnetic field control of plasma boundary locations and atmospheric loss: Mhd prediction and comparison with maven. *J. Geophys. Res. Space Phys.* 122, 4117–4137. doi:10.1002/2016ja023509

Fowler, C. M., McFadden, J., Hanley, K. G., Mitchell, D. L., Curry, S., and Jakosky, B. (2022). *In-situ* measurements of ion density in the martian ionosphere: Underlying structure and variability observed by the MAVEN-STATIC instrument. *J. Geophys. Res. Space Phys.* 127 (8). doi:10.1029/2022JA030352

Gao, J., Rong, Z. J., Klinger, L., Li, X. Z., and Wei, Y. (2021). A spherical harmonic Martian crustal magnetic field model that combines MAVEN and MGS data. *Earth Space Sci.* 8, e2021EA001860. doi:10.1029/2021EA001860

Garnier, P., Jacquey, C., Gendre, X., Génot, V., Mazelle, C., Fang, X., et al. (2022). The drivers of the martian bow shock location: A statistical analysis of mars atmosphere and volatile EvolutioN and mars express observations. *J. Geophys. Res. Space Phys.* 127 (5), e2021JA030147. doi:10.1029/2021JA030147

Girazian, Z., Mahaffy, P. R., Lillis, R. J., Benna, M., Elrod, M., and Jakosky, B. M. (2017). Nightside ionosphere of Mars: Composition, vertical structure, and variability. *J. Geophys. Res. Space Phys.* 122, 4712–4725. doi:10.1002/2016JA023508

Huestis, D. L. (2001). Accurate evaluation of the Chapman function for atmospheric attenuation. *J. Quantitative Spectrosc. Radiat. Transf.* 69 (6), 709–721. doi:10.1016/S0022-4073(00)00107-2

Inui, S., Seki, K., Sakai, S., Brain, D., Hara, T., McFadden, J., et al. (2021). Statistical study of heavy ion outflows from mars observed in the martian-induced magnetotail by MAVEN. *J. Geophys. Res. Space Phys.* 124 (7), 5482–5497. doi:10.1029/2018ja026452

Li, S., Lu, H., Cao, J., Cui, J., Zhou, C., Wild, J. A., et al. (2022b). Deflection of O_2^+ ion flow by magnetic fields in the martian ionosphere. *Astrophysical J.* 941, 198. doi:10.3847/1538-4357/aca32b

Li, S., Lu, H., Cao, J., Mazelle, C., Cui, J., Rong, Z., et al. (2022a). The impact and mechanism of the magnetic inclination angle on O^+ escape from Mars. *Astrophysical J.* 931 (30), 30. doi:10.3847/1538-4357/ac6510

Li, S., Lu, H., Cui, J., Yu, Y., Mazelle, C., Li, Y., et al. (2020). Effects of a dipole-like crustal field on solar wind interaction with Mars. *Earth Planet. Phys.* 4 (1), 1–9. doi:10.26464/epp2020005

Li, Y., Lu, H., Cao, J., Li, S., Mazelle, C., and Li, G. (2021). Three-dimensional multispecies simulation of the solar wind interaction with mars under different interplanetary magnetic field orientations. *Astrophysical J.* 921 (2), 139. doi:10.3847/1538-4357/ac1ce5

Liu, D., Rong, Z., Gao, J., He, J., Klinger, L., Dunlop, M. W., et al. (2021). Statistical properties of solar wind upstream of mars: MAVEN observations. *Astrophysical J.* 911 (113), 113. doi:10.3847/1538-4357/abed50

Liu, D., Yao, Z., Wei, Y., Rong, Z., Shan, L., Arnaud, S., et al. (2020). Upstream proton cyclotron waves: Occurrence and amplitude dependence on IMF cone angle at mars — From MAVEN observations. *Earth Planet. Phys.* 4 (1), 51–11. doi:10.26464/epp2020002

Luhmann, J. G., Dong, C. F., Ma, Y. J., Curry, S. M., Xu, S., Lee, C. O., et al. (2017). Martian magnetic storms. *J. Geophys. Res. Space Phys.* 122, 6185–6209. doi:10.1002/2016JA023513

Lundin, R., Barabash, S., Yamauchi, M., Nilsson, H., and Brain, D. (2011). On the relation between plasma escape and the martian crustal magnetic field. *Geophys. Res. Lett.* 38 (2), L02102. doi:10.1029/2010gl046019

Lundin, R., Winningham, D., Barabash, S., Frahm, R., Holmström, M., Sauvaud, J. A., et al. (2006). Plasma acceleration above martian magnetic anomalies. *Science* 311 (5763), 980–983. doi:10.1126/science.1122071

Ma, Y., Nagy, A. F., Sokolov, I. V., and Hansen, K. C. (2004). Three-dimensional, multispecies, high spatial resolution mhd studies of the solar wind interaction with Mars. *J. Geophys. Res. Space Phys.* 109 (A7), A07211. doi:10.1029/2003JA010367

Ma, Y. J., Fang, X., Russell, C. T., Nagy, A. F., Toth, G., Luhmann, J. G., et al. (2014). Effects of crustal field rotation on the solar wind plasma interaction with Mars. *Geophys. Res. Lett.* 41 (19), 6563–6569. doi:10.1002/2014GL060785

Ma, Y. J., Russell, C. T., Fang, X., Dong, Y., Nagy, A. F., Toth, G., et al. (2015). MHD model results of solar wind interaction with Mars and comparison with maven plasma observations. *Geophys. Res. Lett.* 42 (21), 9113–9120. doi:10.1002/2015gl065218

Matta, M., Mendillo, M., Withers, P., and Morgan, D. (2015). Interpreting Mars ionospheric anomalies over crustal magnetic field regions using a 2-d ionospheric model. *J. Geophys. Res. Space Phys.* 120, 766–777. doi:10.1002/2014ja020721

Nagy, A. F., Winterhalter, D., Sauer, K., Cravens, T., Brecht, S., Mazelle, C., et al. (2004). The plasma environment of Mars. *Space Sci. Rev.* 111 (1), 33–114. doi:10.1023/b:spac.0000032718.47512.92

Nilsson, H., Edberg, N. J., Stenberg, G., Barabash, S., Holmström, M., Futaana, Y., et al. (2011). Heavy ion escape from Mars, influence from solar wind conditions and crustal magnetic fields. *Icarus* 215 (2), 475–484. doi:10.1016/j.icarus.2011.08.003

Sánchez-Cano, B., Narvaez, C., Lester, M., Mendillo, M., Mayyasi, M., Holmstrom, M., et al. (2020). Mars' ionopause: A matter of pressures. *J. Geophys. Res. Space Phys.* 125 (9). doi:10.1029/2020JA028145

Ulusen, D., Luhmann, J., Ma, Y., and Brain, D. (2016). Solar control of the Martian magnetic topology: Implications from model-data comparisons. *Planet. Space Sci.* 128, 1–13. doi:10.1016/j.pss.2016.01.007

Vignes, D., Mazelle, C., Rme, H., Acuña, M. H., Connerney, J. E. P., Lin, R. P., et al. (2000). The solar wind interaction with mars: Locations and shapes of the bow shock and the magnetic pile-up boundary from the observations of the MAG/ER experiment onboard mars global surveyor. *Geophys. Res. Lett.* 27 (1), 49–52. doi:10.1029/1999GL010703

Weber, T., Brain, D., Mitchell, D., Xu, S., Connerney, J., and Halekas, J. (2017). Characterization of low-altitude nightside Martian magnetic topology using electron pitch angle distributions. *J. Geophys. Res. Space Phys.* 122, 9777–9789. doi:10.1002/2017JA024491

Weber, T., Brain, D., Mitchell, D., Xu, S., Espley, J., Halekas, J., et al. (2019). The influence of solar wind pressure on Martian crustal magnetic field topology. *Geophys. Res. Lett.* 46, 2347–2354. doi:10.1029/2019GL081913

Weber, T., Brain, D., Xu, S., Mitchell, D., Espley, J., Halekas, J., et al. (2020). The influence of interplanetary magnetic field direction on Martian crustal magnetic field topology. *Geophys. Res. Lett.* 47. doi:10.1029/2020GL087757

Withers, P. (2009). A review of observed variability in the dayside ionosphere of Mars. *Adv. Space Res.* 44 (3), 277–307. doi:10.1016/j.asr.2009.04.027

Xu, S., Fang, X., Mitchell, D. L., Ma, Y., Luhmann, J. G., DiBraccio, G. A., et al. (2018). Investigation of Martian magnetic topology response to 2017 September ICME. *Geophys. Res. Lett.* 45, 7337–7346. doi:10.1029/2018GL077708

Xu, S., Liemohn, M. W., Dong, C., Mitchell, D. L., Bougher, S. W., and Ma, Y. (2016). Pressure and ion composition boundaries at Mars. *J. Geophys. Res. Space Phys.* 121 (7), 6417–6429. doi:10.1002/2016ja022644

Xu, S., Mitchell, D., Liemohn, M., Fang, X., Ma, Y., Luhmann, J., et al. (2017). Martian low-altitude magnetic topology deduced from MAVEN/SWEA observations. *J. Geophys. Res. Space Phys.* 122 (2), 1831–1852. doi:10.1002/2016ja023467

Xu, S., Weber, T., Mitchell, D. L., Brain, D. A., Mazelle, C., DiBraccio, G. A., et al. (2019). A technique to infer magnetic topology at Mars and its application to the terminator region. *J. Geophys. Res. Space Phys.* 124, 1823–1842. doi:10.1029/2018JA026366

Yao, Z. H., Murphy, K. R., Rae, I. J., and Balan, N. (2017). Introduction to the thematic series "Coupling of the magnetosphere–ionosphere system. *Geosci. Lett.* 4, 27. doi:10.1186/s40562-017-0092-5

Zhang, C., Rong, Z., Klinger, L., Nilsson, H., Shi, Z., He, F., et al.(2022). Three-dimensional configuration of induced magnetic fields around Mars. *J. Geophys. Res. Planets* 127, e2022JE007334. doi:10.1029/2022JE007334